JTTEE5 13:370-376
DOI: 10.1361/10599630420380
1059-9630/$19.00 © ASM International

Peer Reviewed

The Effect of a High Thermal Gradient on Sintering and Stiffening in the Top Coat of a Thermal Barrier Coating System

S.A. Tsipas, I.O. Golosnoy, R. Damani, and T.W. Clyne

(Submitted October 30, 2003; in revised form December 3, 2003)

Superalloy substrates coated with plasma-sprayed CoNiCrAlY bond coats and yttria-stabilized zirconia top coats (TCs) have been subjected to a high heat flux under a controlled atmosphere. The sintering exhibited by the TC under these conditions has been studied and compared with the behavior observed during isothermal heating. Sintering has been characterized by (a) microstructural examinations, (b) dilatometry, in both the in-plane and through-thickness directions, and (c) stiffness measurements, using both cantilever bending and nanoindentation. A numerical model has been used to explore the stress state under isothermal and thermal gradient conditions. Dilatometry data indicate significant linear contractions during holding at elevated temperatures, particularly in the through-thickness direction. This is largely attributed to microstructural changes associated with sintering, with any volume changes due to phase transformations making relatively small contributions. Sintering proceeds faster at higher temperatures but is retarded by the presence of tensile stresses (from differential thermal expansion between the coating and substrate) within the TC. Thus, it occurs preferentially near the free surface of the TC under gradient conditions, not only due to the higher temperature, but also because the in-plane stress is more compressive in that region.

Keywords high thermal gradient, sintering, stiffness, thermal barrier coatings, thermal conductivity

1. Introduction

The failure of thermal barrier coatings (TBCs) commonly occurs as a result of the buckling and spalling of the top coat (TC).[1-7] The strain tolerance of the TC is important, and this has been extensively studied for both electron beam physical vapor deposition (EB-PVD) and plasma-sprayed (PS) systems. For PS TCs, this strain tolerance is enhanced by the high compliance, which is largely a consequence of the presence of many fine microcracks and pores in the microstructure. This low stiffness inhibits the buildup of large stresses and hence limits the driving forces for spallation. Recent work[8-12] has confirmed that, while air PS (APS) and vacuum-plasma-sprayed (VPS) TCs have low in-plane Young's moduli in the as-sprayed state, the stiffness rises substantially during holding at elevated temperatures as a consequence of sintering phenomena. This stiffening will raise the strain energy release rate associated with a given misfit strain and hence will make spallation more likely. Furthermore, sintering also raises the thermal conductivity, reducing the thermal protection provided by the TBC. There also has been extensive previous work on the phase changes[13-15] that take place in PS ZrO_2-Y_2O_3 coatings during exposure to high temperature, and this may be relevant to some aspects of their performance.

S.A. Tsipas, I.O. Golosnoy, and **T.W. Clyne,** Department of Materials Science & Metallurgy, Cambridge University, Pembroke Street, Cambridge CB2 3QZ, UK; and **R. Damani,** Sulzer Innotec, Postfach 65, CH-8404 Winterthur, Switzerland. Contact e-mail: twc10@cam.ac.uk.

It is also important to recognize that service conditions involve the presence of a high through-thickness thermal gradient, which will modify the residual stress distribution. This will affect the driving force for spallation and might also be expected to influence the sintering characteristics. This article is aimed at investigating the thermomechanical stability of TBCs, with particular reference to the effect of a high thermal gradient.

2. Experimental Procedures

2.1 Coating Production

The powders were supplied by Sulzer Metco (Westbury, NY). The bond coat (BC) material, designated Amdry 995/C, has a nominal composition (in wt.%) of Co32Ni-21Cr-8Al-0.5Y. The TC was yttria partially stabilized zirconia (YPSZ) (ZrO_2-7.6 wt.%Y_2O_3), designated 204NS-1. These were deposited onto 50 mm thick Nimonic 80A (Special Metals Limited, Hereford, UK) substrates and mild steel substrates of 1.5 mm thickness. Specimens were produced by VPS of the BC, followed by APS of the TC, using the conditions shown in Table 1. The BCs were about 140 μm in thickness, and the thickness of the TCs varied between about 1.5 and 2.6 mm.

2.2 Heat Treatment

A schematic of the high thermal gradient rig is shown in Fig. 1. The base of the substrate was brazed to a water-cooled copper block. Insulation was placed around the specimen to minimize lateral heat losses. The graphite susceptor could be lifted away from the induction coil by a hydraulic ram, allowing thermal cycling of the specimen. The thermal gradient was monitored and controlled by four thermocouples embedded in the substrate. The temperature in the TC was monitored using a thermocouple that was inserted into a laser-drilled hole parallel to

the BC/TC. The laser-drilled hole was 2 mm deep and was drilled using a pulsed Nd-YAG laser with wavelength λ =1.06 μm, 0.5 ms pulse duration, and energy of 2.5 J per pulse.

The holding time at temperature for each thermal cycle was 1 h, and samples were allowed to cool to room temperature before being reheated. Heating rates were ~20 K/min, and cooling rates were ~30 K/min. Typical TC temperatures during the gradient heat treatments applied in the present work ranged from about 1500 °C at the free surface to 900 °C at the interface. A vacuum of 2×10^{-4} mbar was maintained throughout. Isothermal heat treatments of detached samples in air also were performed at temperatures in the range 1200-1400 °C.

2.3 Dimensional, Stiffness, and Microstructural Changes

2.3.1 Dilatometry. Length changes during heat treatment were measured with a DIL 402C dilatometer (Netzsch, Selb, Germany). Dilatometry was performed on detached TCs, in both the in-plane and through-thickness directions. TCs were first detached from steel substrates using hydrochloric acid.

2.3.2 Stiffness Measurement. Stiffness measurements were made using both cantilever bending and nanoindentation. Details of the cantilever bend testing are given elsewhere.[12]

Table 1 Plasma Spraying Parameters

	Deposit Material	
Spraying Parameters	**CoNiCrAlY**	**ZrO_2-Y_2O_3**
Type of spraying	VPS	APS
Spraying distance, mm	270	105
Arc current, A	500	750
Voltage, V	50	60
Gun speed, mm/s	100	55
Nozzle diameter, mm	8	8
Ar flow rate, L/min	50	50
H_2 flow rate, L/min	10	8
Chamber pressure, mbar	200 (Ar)	1000 (air)

Nanoindentation was carried out on polished transverse sections, using a NanoTest 600 indenter (MicroMaterials Ltd., Wrenham, UK). All indentations were made with a Berkovich diamond indenter. Regions remote from obvious microcracks and pores were chosen for performing indentations. The maximum load was 100 mN, and the loading rate was 5.1 mN/s.

2.3.3 X-Ray Diffraction. X-ray diffraction (XRD) for phase identification and lattice parameter measurement was carried out using a computer-controlled diffractometer (PW3020 diffractometer, Philips, Almelo, The Netherlands), with CuKα radiation (λ = 0.154 nm). The $(400)_{tet}$, $(004)_{tet}$, and $(400)_{cub}$ peak

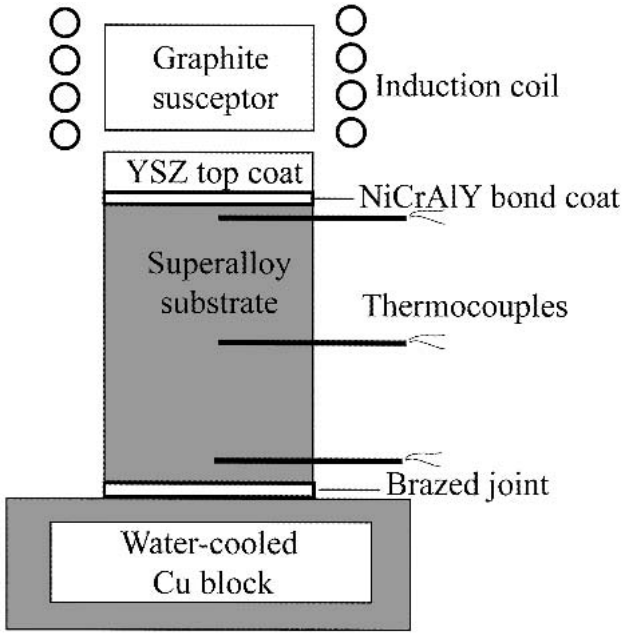

Fig. 1 Schematic illustration of the high thermal gradient rig

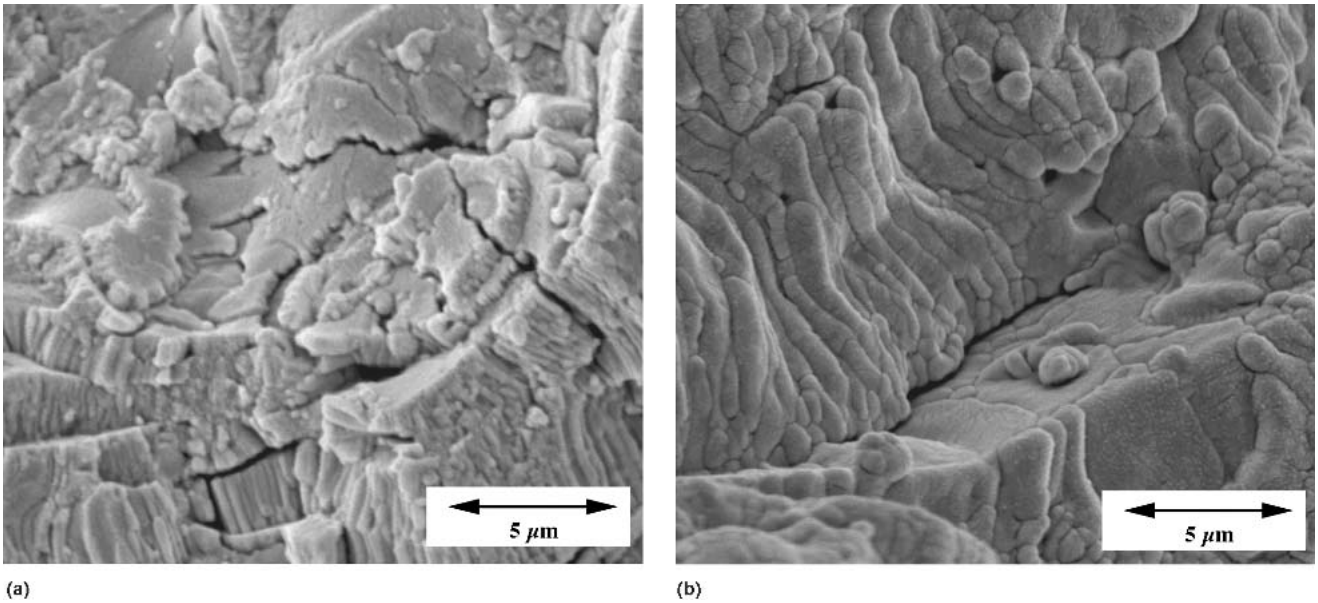

Fig. 2 SEM micrographs of the fracture surfaces of ZrO_2-Y_2O_3 TCs **(a)** as-sprayed and **(b)** after isothermal heat treatment at 1300 °C for 100 h

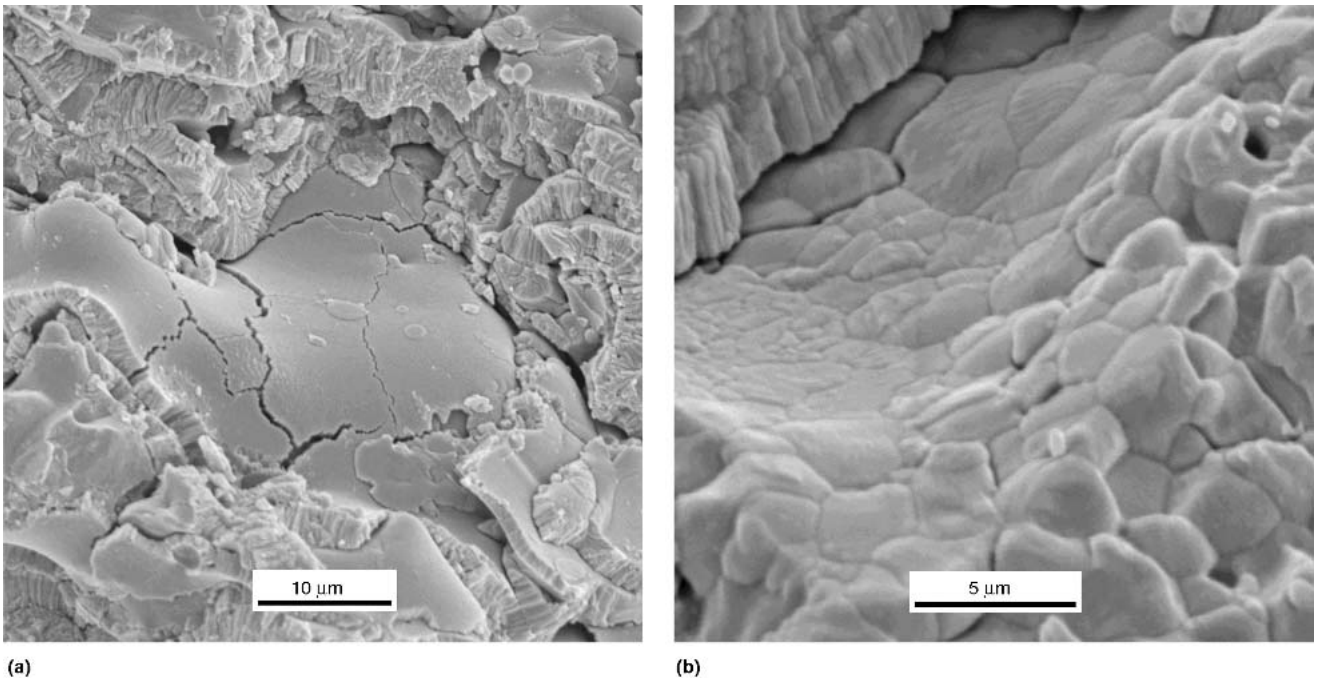

Fig. 3 SEM micrographs of a ZrO_2-Y_2O_3 TC after exposure to a high thermal gradient for 17 h **(a)** near the TC/BC interface and **(b)** near the TC outer surface

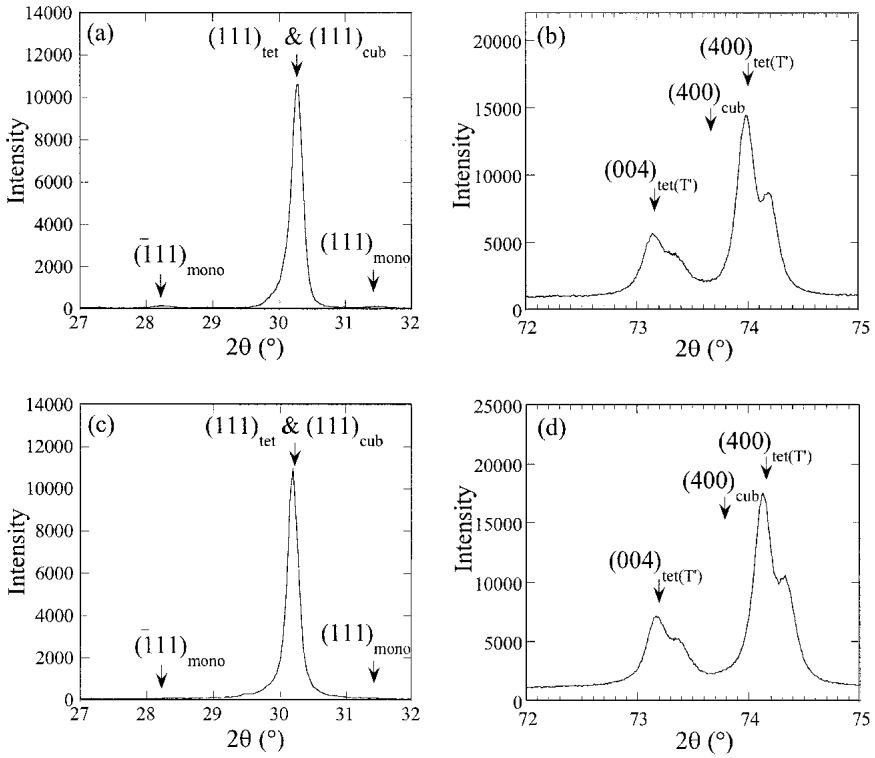

Fig. 4 XRD spectra in the 2θ range 27-32° and 72-75° for ZrO_2-Y_2O_3 TC **(a)** and **(b)** as-sprayed and **(c)** and **(d)** after gradient heat treatment, near the interface with the BC (which was at about 900 °C)

positions were used for the calculation of lattice parameters, *a* for the cubic phase and *a* and *c* for the tetragonal phase. The Y_2O_3 contents of the tetragonal and cubic phases were calculated from these measured lattice parameters, respectively, using the following equations,[16,17] where *a* and *c* are expressed in nanometers:

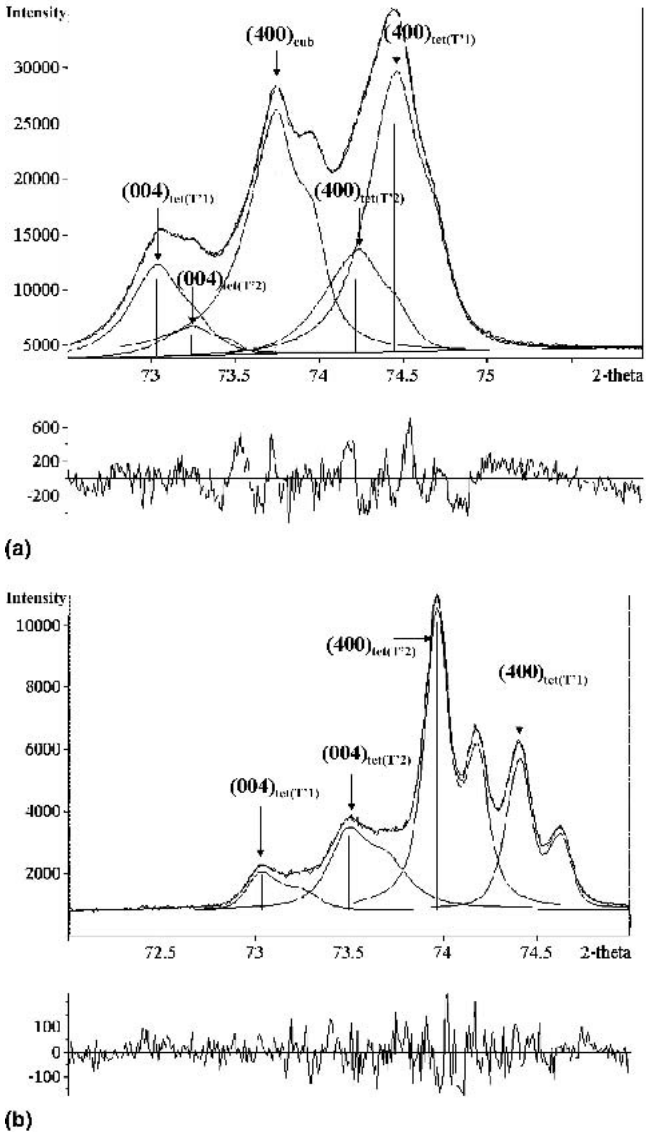

Fig. 5 XRD spectra, with deconvoluted peaks and differential plots (showing the deviation between the measured and modeled spectra). The plots cover the 2θ range 72-75° for ZrO_2-Y_2O_3 TCs, **(a)** after isothermal heat treatment for 100 h at 1300 °C and **(b)** after thermal gradient heat treatment, near the free surface (which was at about 1500 °C).

$$\text{mole\% } YO_{1.5} \text{ in tetragonal phase} = \frac{1.0223 - c/a}{0.001309} \quad \text{(Eq 1)}$$

$$\text{mole\% } YO_{1.5} \text{ in cubic phase} = \frac{a - 0.5104}{0.0204} \quad \text{(Eq 2)}$$

3. Microstructural Changes

3.1 Scanning Electron Microscope Examination

3.1.1 Isothermal Heat Treatment. Figure 2 shows scanning electron microscope (SEM) micrographs of fracture surfaces of YPSZ, before and after heat treatment. As-sprayed coatings exhibit the characteristic splat structure of PS coatings. The grain structure within individual splats is columnar. Microcracks and pores are also present. Heat treatment results in grain growth, often bridging interfaces between splats in close physical proximity. There is also evidence of the healing of through-thickness microcracks.

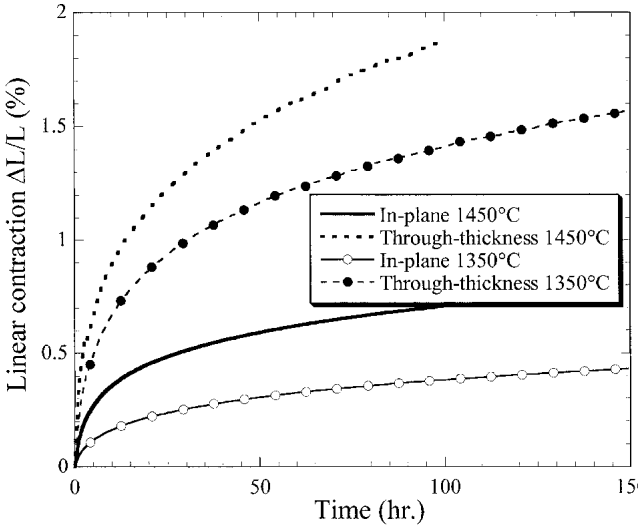

Fig. 6 Dilatometry plots obtained during heat treatment of detached TCs

3.1.2 Heat Treatment With a High Thermal Gradient. Figure 3 shows SEM micrographs of the TC after heat treatment with an imposed thermal gradient. It can be seen that, near the TC/BC interface, there has been little or no sintering. Microcracks are still present, and the bonding between splats is poor. Grains in individual splats have maintained their columnar structure. Near the free surface of the TC, on the other hand, pronounced sintering has taken place. There has been extensive healing of microcracks, and grain growth has occurred, with many grains becoming both larger and more equiaxed in morphology.

3.2 Phase Constitution

XRD spectra are presented in Fig. 4 and 5, covering 2θ ranges in which characteristic peaks appear when the tetragonal, monoclinic, and cubic phases are present. Figure 4 shows that essentially only the nontransformable tetragonal T′ phase is present in the as-sprayed TC. This is also true for the thermal gradient treated material close to the interface with the BC. The $K\alpha_1$ and $K\alpha_2$ components of the T′ peaks can be distinguished. The nontransformable T′ tetragonal phase results from a diffusionless shear transformation directly from the cubic state, due to the rapid cooling of the molten splats during spraying. Just a trace of the monoclinic phase is evident in these scans.

Figure 5(a) shows that, after holding at 1300 °C for 100 h, the tetragonal T′ phase has decomposed to a mixture of low-yttria tetragonal T_1' (deduced from the XRD data to have a composition of 1.7 wt.% Y_2O_3), high-yttria cubic (F) (13 wt.% Y_2O_3), and T_2' with an intermediate composition (6.3 wt.% Y_2O_3). This results from diffusional segregation of the yttria to lower and

Table 2 Measured X-Ray Peak Positions, Deduced Lattice Parameters, and Associated Unit Cell Volumes for Phases Within Coatings, With and Without a Prior Heat Treatment

Phase/Treatment	Tetragonal T′/ As-Sprayed	Tetragonal T_1'/ 100 h at 1300 °C	Tetragonal T_2'/ 100 h at 1300 °C	Cubic F/ 100 h at 1300 °C
2θ for (004) $K\alpha_1$ degrees	73.139	73.030	73.236	…
2θ for (400) $K\alpha_1$ degrees	73.981	74.447	74.217	73.738
c, nm	0.51737	0.51803	0.51678	…
a, nm	0.51231	0.50956	0.51091	0.51375
Y_2O_3, wt.%	7.8	1.7	6.3	13
Vol. of unit cell, nm^3	0.13579	0.13451	0.13489	0.13561
$\Delta V/V$, %	0	−0.94	−0.66	−0.13

Note: Phase compositions deduced from the lattice parameters, using Eq 1 and 2

higher yttria regions, with corresponding changes in the *c/a* ratio.[13] (Of course, it must be recognized that some changes in phase constitution, and possibly in the composition of the phases, will have occurred during cooling to room temperature.) In the thermal gradient treated material near the free surface (which was probably being held at about 1500 °C), on the other hand, the XRD spectrum (Fig. 5b) indicates a mixture of low-yttria and high-yttria tetragonal phases (T_1' and T_2'), having compositions of 2.2 wt.% Y_2O_3 and 11.8 wt.% Y_2O_3, respectively, with no residual cubic phase. It is not entirely clear why no cubic phase survives down to room temperature after holding at about 1500 °C, while quite a significant amount is present after holding at 1300 °C, since the phase diagram indicates that more cubic material should be present at the higher temperature. However, this behavior has been reported[13,15] previously, particularly if the cooling rates were high (as they were in the present work), although no explanation has been put forward for the observation that a higher heat treatment temperature results in less residual cubic phase. One possibility is that, since the cubic phase forming at higher holding temperatures is expected to have a lower yttria composition than if it had formed at lower temperatures, this may render it more liable to transform during rapid cooling.

3.3 Dilatometry

Dilatometry data are presented in Fig. 6. The linear contraction is plotted against time at temperature. Contraction (shrinkage) occurs due to sintering of the coatings. For a given direction, the sintering is faster at higher temperature, and in all cases the rate of contraction falls off with time. These results are broadly consistent with those of previous studies of sintering in TCs[18-21] and of rates of stiffness change.[12,22] It is also clear that more contraction occurs in the through-thickness direction than in the in-plane direction. This effect does not appear to have been reported previously for PS zirconia, although anisotropic shrinkage has been observed for PS alumina.[23] The results suggest that the intersplat spacing in the through-thickness direction is reduced as splats sinter together. The effect is less pronounced in the in-plane directions as a result of the high aspect ratio of the splats.

3.4 Effect of Phase Transformations on Measured Volume Changes

An estimate can be made of the magnitude of the volume changes associated with relevant phase changes, or at least an upper bound can be placed on them. There is particular interest in the tetragonal-to-cubic transformation, since this is likely to occur during extended heating at high temperature. This can be seen from the phase diagram.[17] An upper bound on the expected volume change can be obtained by assuming that thermodynamic equilibrium is attained at the heat treatment temperature. For example, at ~1300 °C, up to ~50% of the tetragonal phase could be transformed to the cubic phase, for material with an overall composition of about ZrO_2-7 wt.%Y_2O_3. Since the number of atoms per unit cell is the same for (all of the possible) tetragonal and cubic phases, it is only necessary to establish the volume of the unit cell in each case, which can be obtained using lattice parameter values inferred from measured x-ray peak positions.* The composition also can be deduced from these measured lattice parameters (using Eq 1 and 2), although it may be noted that the atomic weights of Zr and Y are so close that it is not really necessary to take account of the composition when estimating phase densities from lattice parameter data. Measured peak positions, lattice parameters, and unit cell volumes are given in Table 2. It can be seen that a volume contraction of up to about 0.5-0.6% might be expected when tetragonal material containing about 7 wt.% Y_2O_3 transforms to 50% of F phase containing 13 wt.% Y_2O_3 and to 50% of T_1' phase containing 2 wt.% Y_2O_3. The corresponding linear contraction is thus about 0.2%. It can be concluded that phase changes are expected to make only relatively small contributions to dilatometry data, indicating linear contractions of the order of 1% or more. Thus, these can be attributed primarily to microstructural changes associated with sintering effects. If anything, the effect of taking phase transformation-induced linear contraction into account would be to increase the deduced anisotropy of the sintering contraction.

4. Mechanical Characteristics

4.1 Stiffness Measurements

4.1.1 Cantilever Bending. This technique, which measures the global in-plane stiffness of the coating, was applied to detached, as-sprayed TCs. The value obtained was 10 ± 5 GPa.

*Of course, the x-ray data were obtained at room temperature, whereas interest centers on the volume achieved at high temperature. However, the difference in thermal expansion values between the cubic and tetragonal phases was apparently[24] less than 1×10^6 K^{-1}, so the possible error from this source must be less than about 0.1% in linear dimensions.

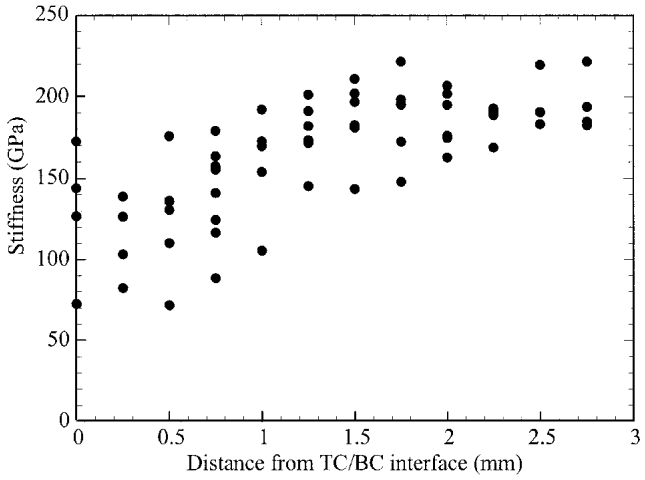

Fig. 7 Stiffness data obtained by nanoindentation on a polished transverse section of a TC after heat treatment in a thermal gradient (~900 °C at the interface, ~1500 °C at the free surface) for 17 h

This was found to increase to around 60 ± 10 GPa after a heat treatment of about 100 h at 1300 °C. It is known that the stiffness of these materials varies with the applied stress level, tending to be higher under compressive loading, which closes the microcracks. In the present work, the applied stresses were in the range ±10 MPa, with associated strains of up to about ±1 millistrain. In the results presented here, this effect is neglected, but it may be noted that the resultant error in stiffness is probably[25] of the order of ±5 GPa. This is a significant uncertainty, but the observed trend of increasing stiffness after heat treatment is nevertheless quite clear.

4.1.2 Nanoindentation. Measurements were made on a TC that had been heat treated for 17 h with a high thermal gradient. The data are shown in Fig. 7. A through-thickness gradient in the stiffness is apparent. Near the TC/BC interface, values were similar to those obtained with the as-sprayed TC, but near the outer surface the average value increases, approaching that of monolithic dense YSZ. There is, of course, quite a lot of scatter in the data, since the value obtained is sensitive to the presence or absence of neighboring fine-scale flaws. These results are consistent with the microstructural observations, indicating pronounced sintering near the outer surface. The absolute values of Young's modulus obtained using this technique are, as expected, much higher than those given by methods that measure the global stiffness, since gross flaws affect the latter, but not the former. Also, the indentation method senses the compressive stiffness only, which is known to be larger than that achieved under tension in these materials, particularly at relatively high strains.

4.2 Stress State During Heat Treatment

A model developed by Clyne and coworkers[26-30] has been used in the present work for the prediction of residual stresses after spraying and subsequent heat treatments. The predicted effect of imposing a high through-thickness thermal gradient is shown in Fig. 8. It can be seen that the stress level in the coating is moved toward more compressive values when the thermal gradient is imposed, particularly near the free surface. This is

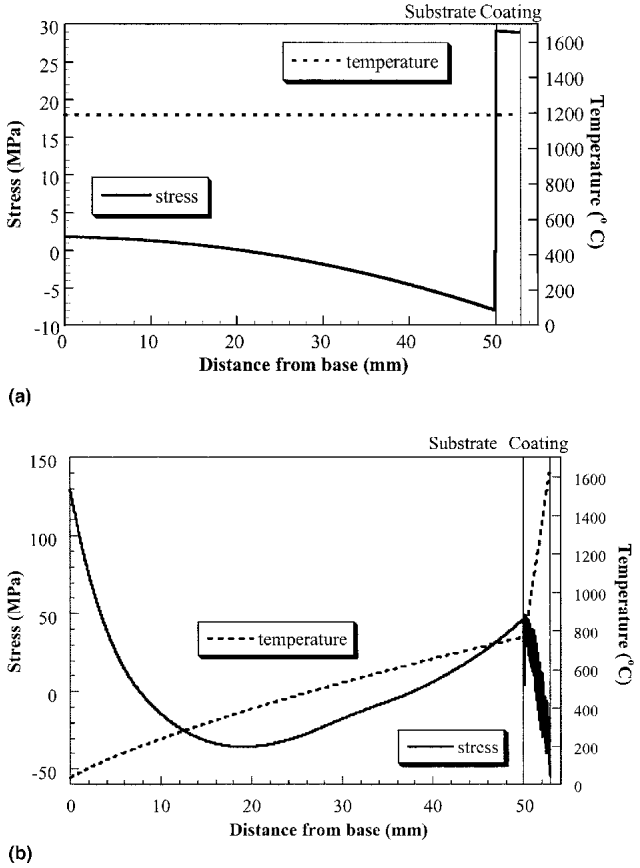

Fig. 8 Predicted through-thickness distributions of stress and temperature in a TBC system **(a)** when isothermal at 1200 °C and **(b)** when subjected to a high thermal gradient, similar to that used in the experimental work

expected to accelerate the rates of sintering and stiffening, since it is now well established[12] that these processes are retarded by the presence of tensile stresses, which hold open the microcracks and pores.

5. Conclusions

The following conclusions can be drawn from this work.

- Detached TCs exhibit substantial reductions in linear dimensions during holding at elevated temperatures. These linear contractions are greater in the through-thickness direction than in the in-plane directions. This is thought to be at least primarily associated with microstructural changes induced by sintering processes, and the anisotropy is a consequence of the splat and pore geometry in these coatings. Any contributions arising from phase changes occurring at high temperature are expected to be relatively small.
- The high thermal gradients commonly present in TBCs under service conditions lead to widely varying conditions within the TC. Sintering is likely to occur much more rapidly near the free surface, not only because the temperatures are higher there, but because the residual stresses tend to be

more compressive. It is known that tensile stresses retard the progression of sintering.

- Exposure to high temperatures near the free surface also can induce phase changes, which may affect the microstructure and perhaps the stress state. The as-sprayed TC is entirely the so-called nontransformable tetragonal T′ phase. Isothermal heat treatment at 1300 °C generates material with a significant proportion of the cubic (F) phase. After heat treatment in a high thermal gradient, material near the BC remained entirely composed of T′, whereas material near the free surface was composed of a mixture of low-yttria and high-yttria tetragonal phases (T'_1 and T'_2), which were formed on cooling from the high-temperature tetragonal (T′) and cubic (F) phases, respectively.

Acknowledgments

Funding for this work has come from Engineering and Physical Sciences Research Laboratory, which has had Rolls Royce and Sulzer Corp. as industrial partners, in the form of a Platform Grant and a research project. One of the authors (SAT) also has received financial support from the Cambridge European Trust. There have been many useful discussions with industrial partners, particularly Jason Doesburg, Andrew Nicoll, and Keith Harrison (Sulzer Metco). The collaboration of Prof. Richard Jones, from Defense Science and Technology Laboratory, has also been very helpful.

References

1. M.P. Taylor, P. Niranatlumpong, H.E. Evans, and C.B. Ponton: "Observations of the Spallation Modes in an Overlay Coating and the Corresponding Thermal Barrier Coating System," *Mater. High Temp.,* 2000, *17,* pp. 219-24.
2. J. Rosler, M. Baker, and M. Volgmann: "Stress State and Failure Mechanisms of Thermal Barrier Coatings: Role of Creep in Thermally Grown Oxide," *Acta Mater.,* 2001, *49,* pp. 3659-70.
3. A.G. Evans, D.R. Mumm, J.W. Hutchinson, G.H. Meier, and F.S. Pettit: "Mechanisms Controlling the Durability of Thermal Barrier Coatings," *Prog. Mater. Sci.,* 2001, *46,* pp. 505-53.
4. R.A. Handoko, J.L. Beuth, G.H. Meier, F.S. Pettit, and M.J. Stiger: "Mechanisms for Interfacial Toughness Loss in Thermal Barrier Coating Systems," *Key Eng. Mater.,* 2001, *197,* pp. 165-83.
5. T. Vogt, B.A. Hunter, and J. Thornton: "Structural Evolution of Thermal-Sprayed Yttria-Stabilized ZrO2 Thermal Barrier Coatings With Annealing: A Neutron Diffraction Study," *J. Am. Ceram. Soc.,* 2001, *84,* pp. 678-80.
6. R. Vassen, G. Kerkhof, and D. Stover: "Development of a Micromechanical Life Prediction Model for Plasma Sprayed Thermal Barrier Coatings," *Mater. Sci. Eng. A Struct.,* 2001, *303,* pp. 100-09.
7. J.W. Hutchinson and A.G. Evans: "On the Delamination of Thermal Barrier Coatings in a Thermal Gradient," *Surf. Coat. Technol.,* 2002, *149,* pp. 179-84.
8. P.A. Langjahr, R. Oberacker, and M.J. Hoffmann: "Long-Term Behaviour and Application Limits of Plasma-Sprayed Zirconia Thermal Barrier Coatings," *J. Am. Ceram. Soc.,* 2001, *84,* pp. 1301-08.
9. D.M. Zhu and R.A. Miller: "Thermal Conductivity and Elastic Modulus Evolution of Thermal Barrier Coatings under High Heat Flux Conditions," *J. Thermal Spray Technol.,* 2000, *9,* pp. 175-80.
10. R. Dutton, R. Wheeler, K.S. Ravichandran, and K. An: "Effect of Heat Treatment on the Thermal Conductivity of Plasma-Sprayed Thermal Barrier Coatings," *J. Thermal Spray Technol.,* 2000, *9,* pp. 204-09.
11. D. Basu, C. Funke, and R.W. Steinbrech: "Effect of Heat Treatment on Elastic Properties of Separated Thermal Barrier Coatings," *J. Mater. Res.,* 1999, *14,* pp. 4643-50.
12. J.A. Thompson and T.W. Clyne: "The Effect of Heat Treatment on the Stiffness of Zirconia Top Coats in Plasma-Sprayed TBCs," *Acta Mater.,* 2001, *49,* pp. 1565-75.
13. J. Brandon and R.Taylor: "Phase Stability of Zirconia-Based Thermal Barrier Coatings: Part I. Zirconia-Yttria Alloys," *Surf. Coat. Technol.,* 1991, *46,* pp. 75-90.
14. R.W. Trice, Y.J. Su, J.R. Mawdsley, K.T. Faber, A.R. De Arellano-Lopez, H. Wang, and W.D. Porter: "Effect of Heat Treatment on Phase Stability, Microstructure, and Thermal Conductivity of Plasma-Sprayed YSZ," *J. Mater. Sci.,* 2002, *37,* pp. 2359-65.
15. J. Moon, H. Choi, H. Kim, and C. Lee: "The Effects of Heat Treatment on the Phase Transformation Behavior of Plasma-Sprayed Stabilized ZrO2 Coatings," *Surf. Coat. Technol.,* 2002, *155,* pp. 1-10.
16. R.A. Miller, J.L. Smialek, and R.G. Garlick: "Phase Stability in Plasma-Sprayed, Partially Stabilized Zirconia-Yttria" in *Proceedings of First International Conference on the Science and Technology of Zirconia,* A.H. Heuer and L.W. Hobbs, ed., American Ceramic Society, Westerville, OH, 1980, pp. 241-53.
17. H.G. Scott: "Phase Relationships in the ZrO_2-Y_2O_3 System," *J. Mater. Sci.,* 1975, *10,* pp. 1527-35.
18. H.E. Eaton and R.C. Novak: "Sintering Studies of Plasma Sprayed Zirconia," *Surf. Coat. Technol.,* 1987, *32,* pp. 227-36.
19. D.M. Zhu and R.A. Miller: "Sintering and Creep Behaviour of Plasma-Sprayed Zirconia- and Hafnia-Based Thermal Barrier Coatings," *Surf. Coat. Technol.,* 1998, *109,* pp. 114-20.
20. I.R. Gibson, G.P. Dransfield, and J.T.S. Irvine: "Sinterability of Commercial 8 mol% Yttria-Stabilized Zirconia Powders and the Effect of Sintered Density on the Ionic Conductivity," *J. Mater. Sci.,* 1998, *33,* pp. 4297-4305.
21. R. Vassen, N. Czech, W. Mallener, W. Stamm, and D. Stoever: "Influence of Impurity Content and Porosity of Plasma-Sprayed Yttria-Stabilized Zirconia Layers on the Sintering Behaviour," *Surf. Coat. Technol.,* 2001, *141,* pp. 135-40.
22. J.A. Thompson and T.W. Clyne: "The Stiffness of Plasma Sprayed Zirconia Top Coats in TBCs," in *Proceedings of United Thermal Spray Conference,* E. Lugscheider and P.A. Kammer, ed., DVS, Dusseldorf, Germany, 1999, pp. 835-40.
23. R.J. Damani and P. Makroczy: "Heat Treatment Induced Phase and Microstructural Development in Bulk Plasma Sprayed Alumina," *J. Eur. Ceram. Soc.,* 2000, *20,* pp. 867-88.
24. F. Cardarelli: *Materials Handbook: A Concise Desktop Reference,* Springer-Verlag, London, UK, 2000.
25. J. Malzbender and R.W. Steinbrech: "Mechanical Methods to Determine Layer Compliances Within Multilayered Composites," *J. Mater. Res.,* 2003, *18,* pp. 1374-82.
26. S.C. Gill and T.W. Clyne: "Stress Distributions and Material Response in Thermal Spraying of Metallic and Ceramic Deposits," *Met. Trans.,* 1990, *21B,* pp. 377-85.
27. T.W. Clyne and S.C. Gill: "Heat Flow and Thermal Contraction During Plasma Spray Deposition" in *Heat Transfer in Manufacturing and Processing of New Materials,* I. Tanasawa, ed., Hemisphere, New York, NY, 1991, pp. 33-48.
28. T.W. Clyne and S.C. Gill: "Residual Stresses in Thermally Sprayed Coatings and Their Effect on Interfacial Adhesion: A Review of Recent Work," *J. Thermal Spray Technol.,* 1996, *5,* pp. 1-18.
29. Y.C. Tsui, J.A. Thompson, and T.W. Clyne: "The Effect of Bond Coat Creep on Residual Stresses and Debonding in Plasma Sprayed Thermal Barrier Systems" in *Proceedings of Thermal Spray: Meeting the Challenges of the 21st Century. Proceedings of the 15th International Thermal Spray Conference,* C. Coddet, ed., ASM International, Materials Park, OH, 1998, pp. 1565-70.
30. J.A. Thompson, J. Matejicek, and T.W. Clyne: "Modelling and Neutron Diffraction Measurement of Stresses in Sprayed TBCs" in *Proceedings of Superalloys 2000,* T.M. Pollock, R.D. Kissinger, R.R. Bowman, K.A. Green, M. McLean, S.L. Olsen, and J.J. Schirra, ed., TMS, Warrendale, PA, 2000, pp. 639-47.